J|A|C|S ARTICLES

Published on Web 03/26/2010

Polymetallic Oxalate-Based 2D Magnets: Soluble Molecular Precursors for the Nanostructuration of Magnetic Oxides

Eugenio Coronado,*,† Carlos Martí-Gastaldo,† José R. Galán-Mascarós,‡ and Massimiliano Cavallini§

Instituto de Ciencia Molecular (ICMol), Universidad de Valencia, Polígono de la Coma s/n, 46980 Paterna, Spain, Institute of Chemical Research of Catalonia (ICIQ), Av. Països Catalans 16, 43007 Tarragona, Spain, and CNR-Institute of Nanostructured Materials (ISMN), Via P. Gobetti 101, 40129 Bologna, Italy

Received January 11, 2010; E-mail: eugenio.coronado@uv.es

Abstract: Here we describe the synthesis and magnetic characterization of a family of 2D polymetallic oxalate-bridged polymeric networks with general formula $[M^{II}(H_2O)_2]_3[M^{III}(ox)_3]_2$(18-crown-6)$_2$ (M^{III} = Cr, Fe; M^{II} = Mn, Fe, Co, Ni; 18-crown-6 = $C_{12}H_{24}O_6$). Depending on the nature of the trivalent metal ion, they exhibit ferro- (Cr^{3+}) or ferrimagnetic (Fe^{3+}) ordering in the 3.6−20 K interval. In contrast with most of the oxalate-bridged CPs reported so far, these complexes do not need any additional templating cation for their assembly and represent the first series of oxalate-based polymeric networks which can be considered intrinsically neutral. As previously observed for other crown ether containing oxalate-based coordination polymers, these compounds are soluble in water, whereas they remain nonsoluble in other organic solvents. Furthermore, when these molecular precursors are subjected to a thermally controlled decomposition process, pure phases of mixed oxides with spinel-like structures can be conveniently generated. Among the resulting materials, the $(Mn,Co,Fe)_3O_4$ derivative is particularly remarkable, since it behaves as a magnet at room temperature. Finally, taking advantage of the solubility of these molecular precursors, this room-temperature magnetic oxide has been successfully nanostructured onto a Si(110) substrate via the lithographically controlled wetting (LCW) technique.

Introduction

For the last three decades, molecule-based magnetic materials have demonstrated their ability to mimic and even go beyond the physical properties exhibited by classical inorganic solids.[1] The most successful molecule-based magnets in this "competition" are based in coordination polymers (CPs) composed of transition-metal ions (spin carriers) bridged by small organic ligands able to promote strong enough magnetic exchange.[2] In these molecule-based materials, properties such as flexibility, transparency, low density, and biocompatibility can be combined not only with the magnetism but also with more sophisticated functionalities, thus permitting the design of advanced multifunctional molecular materials such as ferromagnetic conductors,[3] photo and piezo switching magnets,[4] chiral magnets,[5] multiferroics,[6] and hybrid magnets incorporating spin crossover molecules.[7]

Probably one of the most representative ligands to illustrate the versatility of the chemical approach toward the development of this class of materials has been the oxalate linker (ox = $C_2O_4^{2-}$). According to the generally followed bimetallic approach, homoleptic $[M^{III}(ox)_3]^{3-}$ complexes (M^{III} = Cr, Fe, V, Ru, Mn) can be employed as chelating ligands against paramagnetic divalent metal ions, resulting in the formation of discrete oligomeric species which remain in solution because of their charged nature. In a final step, the addition of a cationic molecule promotes the assembling of a layered salt, which can then be isolated from solution. The broad number of magnetic materials obtained through this synthetic route has permitted us to postulate a direct relation between the size, charge, and geometry of the monovalent cation and the dimensionality and symmetry of the resulting oxalate-based architectures. In this way, different cations have templated the formation of different magnetic networks. Whereas alkylic bulky monocations usually lead to the formation of 2D honeycomb-like hexagonal networks exhibiting ferromagnetic, ferrimagnetic, or weak ferromagnetic ordering,[8] the employment of tris-bipyridyl chiral complexes yields homochiral 3D networks which exhibit ferro- and ferrimagnetic ordering at temperatures lower than for their 2D counterparts.[9] More exotic 3D structures with a predominance

† Universidad de Valencia (ICMol).
‡ Institute of Chemical Research of Catalonia (ICIQ).
§ NR-Institute of Nanostructured Materials (ISMN).

(1) (a) Miller, J. S.; Epstein, A. J. *MRS Bull.: Molecule-Based Magnets* **2000**, *25*, 21–28. (b) Miller, J. S. *Adv. Mater.* **1990**, *2*, 98–99.
(2) (a) Day, P.; Underhill, A. E. *Metal-Organic and Organic Molecular Magnets*; Royal Society of Chemistry: Cambridge, U.K., 2000; Spec. Publ. R. Soc. Chem. Vol. 252. (b) Kurmoo, M. *Chem. Soc. Rev.* **2009**, *38*, 1353–1379.
(3) Coronado, E.; Galán-Mascarós, J. R.; Gómez-García, C. J.; Laukhin, V. *Nature* **2000**, *408*, 447–449.
(4) (a) Bénard, S.; Yu, P.; Audiére, J. P.; Riviére, V.; Clèment, R.; Ghilhelm, J.; Tchertanov, L.; Nakatani, K. *J. Am. Chem. Soc.* **2000**, *122*, 9444–9454. (b) Sato, O.; Iyoda, T.; Fujishima, A.; Hashimoto, K. *Science* **1996**, *272*, 704–705. (c) Bleuzen, A.; Lomenech, C.; Escax, V.; Villain, F.; Varret, F.; Cartier, C.; Verdaguer, M. *J. Am. Chem. Soc.* **2000**, *122*, 6648–6652. (d) Coronado, E.; Giménez-López, M. C.; Korzeniak, T.; Levchenko, G.; Romero, F. M.; Segura, A.; García-Baonza, V.; Cezar, J. C.; de Groot, F. M. F.; Milner, A.; Paz-Pasternak, M. *J. Am. Chem. Soc.* **2008**, *130*, 15519–15532.

10.1021/ja100261z

of antiferromagnetic interactions can be also prepared by introducing organic radicals of the nitronyl nitroxide type.[10] Moreover, we recently demonstrated how the combination of two different cations in a layered material permitted us to observe the single chain magnet behavior of an oxalate-based chain for the first time, as result of the strict control on the intensity of the dipolar interactions operating between the layers in the solid state.[11] In this same direction, we have extensively studied the introduction of the planar $[K(18\text{-crown-}6)]^+$ complex (18-crown-6 = $C_{12}H_{24}O_6$) in oxalate-based magnetic materials and illustrated how it promotes a reduction in their dimensionality, leading to less connected 2D anionic layers and even 1D systems, when their growth is assisted with auxiliary capping ligands.[12] These systems also behave as bulk magnets, though at lower temperatures than for their 2D counterparts.

These examples stress the templating role played by the cationic molecule and, which is more important, the essential value of couloumbic interactions in directing the assembling of the molecular species in solution and determining the dimensionality and physical properties of the resulting oxalate-based CP. In our opinion the development of novel, even more complex oxalate-bridged magnetic topologies should be feasible through controlling not only covalent bonding or anion/cation electrostatic interactions but also the less intense but equally determinant supramolecular interactions. In this regard, the importance of hydrogen-bonding interactions in the construction of oxalate-based magnets was recently pointed out in a 2D ferromagnet formed by neutral bimetallic layers: $\{[Co(H_2O)_2]_3[Cr(ox)_3]_2(18\text{-crown-}6)_2\}$.[13] In this system the templating role, typically attributed to cationic moieties, was effectively substituted by the presence of hydrogen-bonding interactions between the neutral crown ether molecule guest and the oxalate-bridged bimetallic neutral CP host, thus constituting the first example of an intrinsically neutral "cation-less" oxalate-based magnet. In the first part of this work we will show how this synthetic strategy can be extended to different paramagnetic metal ions, leading to a family of 2D layered magnets with the general formula $\{[M^{II}(H_2O)_2]_3[M^{III}(ox)_3]_2(18\text{-crown-}6)_2\}$ (M^{III} = Cr, Fe; M^{II} = Mn, Fe, Co, Ni). In the second part, according to the "molecules-to-materials" route previously described for other oxalate complexes,[14] we will show how these molecular materials can be subjected to controlled thermal decomposition, generating pure phases of crystalline mixed oxides with spinel-like structures, which behave as bulk magnets even at room temperature. Finally, the solubility in water of these molecular oxalate-based precursors will be exploited to accomplish the organization of magnetic oxides in the nanoscale using the lithographically controlled wetting (LCW) technique, an unconventional lithographic method[15] which has already been successfully applied to other magnetic hybrid materials.[16]

Experimental Section

Synthesis. All chemicals ($H_2C_2O_4$, $Na_2C_2O_4 \cdot H_2O$, $K_2Cr_2O_7$, $AgNO_3$, $TlNO_3$, $MnCl_2 \cdot 4H_2O$, $FeCl_2 \cdot 4H_2O$, $CoCl_2 \cdot 6H_2O$, $NiCl_2 \cdot 6H_2O$, $CuCl_2 \cdot 2H_2O$, 18-crown-6) and solvents (water, methanol) used were of commercially available grade and were used without any previous purification. $K_3[M^{III}(ox)_3]$ (M^{III} = Cr, Fe) complexes were prepared according to previously described methods.[17] The $Ag_3[Cr(ox)_3]$ derivative was obtained by metathesis of the potassium salt as follows: $K_3[Cr(ox)_3]$ (3 mmol; 1.30 g) was dissolved in the minimum amount of water. Simultaneously, a saturated aqueous solution of $AgNO_3$ (4 mmol; 0.67 g) was prepared and subsequently added to the $K_3[Cr(ox)_3]$ solution. In a few minutes quantitative precipitation of the $Ag_3[Cr(ox)_3]$ complex was observed. The purple

(5) (a) Minguet, M.; Luneau, D.; Lhotel, E.; Villar, V.; Paulsen, C.; Amabilino, D. B.; Veciana, J. *Angew. Chem., Int. Ed.* **2002**, *41*, 586–589. (b) Inoue, K.; Kikuchi, K.; Ohba, M.; Okawa, H. *Angew. Chem., Int. Ed.* **2003**, *42*, 4810–4813. (c) Coronado, E.; Galán-Mascaŕos, J. R.; Gómez-García, C. J.; Murcia-Martínez, A. *Chem. Eur. J.* **2006**, *12*, 3484–3492. (d) Train, C.; Gheorge, R.; Krstic, V.; Chamoreau, L.-M.; Ovanesyan, N. S.; Rikken, G. L. J. A.; Gruselle, M.; Verdaguer, M. *Nat. Mater.* **2008**, *7*, 729–734. (e) Train, C.; Nuida, T.; Gheorghe, R.; Gruselle, M.; Ohkoshi, S. *J. Am. Chem. Soc.* **2009**, *131*, 16838–16843.

(6) Ohkoshi, S.; Tokoro, H.; Matsuda, T.; Takahashi, H.; Irie, H.; Hashimoto, K. *Angew. Chem., Int. Ed.* **2007**, *46*, 3238–3241.

(7) (a) Floquet, S.; Salunke, S.; Boillot, M.-L.; Clément, R.; Varret, F.; Boukheddaden, K.; Rivière, E. *Chem. Mater.* **2002**, *14*, 4164–4171. (b) Floquet, S.; Muñoz, M. C.; Rivière, E.; Clément, R.; Audière, J. P.; Boillot, M. L. *New J. Chem.* **2004**, *28*, 535–541. (c) Clemente-León, M.; Coronado, E.; Giménez-López, M. C.; Soriano-Portillo, A.; Waerenborgh, J. C.; Delgado, F. S.; Ruiz-Pérez, C. *Inorg. Chem.* **2008**, *47*, 9111–9120.

(8) (a) Tamaki, H.; Zhong, Z. J.; Matsumoto, N.; Kida, S.; Koikawa, M.; Achiwa, N.; Hashimoto, Y.; Okawa, H. *J. Am. Chem. Soc.* **1992**, *114*, 6974–6979. (b) Okawa, H.; Matsumoto, N.; Tamaki, H.; Ohba, M. *Mol. Cryst. Liq. Cryst.* **1993**, *232*, 617–622. (c) Tamaki, H.; Mitsumi, M.; Nakamura, K.; Matsumoto, N.; Kida, S.; Okawa, H.; Iijima, S. *Chem. Lett.* **1992**, 1975–1978. (d) Mathoniere, C.; Carling, S. G.; Dou, Y. S.; Day, P. *J. Chem. Soc., Chem. Commun.* **1994**, 1551–1552. (e) Mathoniere, C.; Nuttall, C. J.; Carling, S. G.; Day, P. *Inorg. Chem.* **1996**, *35*, 1201–1206. (f) Coronado, E.; Galan-Mascarós, J. R.; Gómez-García, C. J.; Martínez-Agudo, J. M.; Martínez-Ferrero, E.; Waerenborgh, J. C.; Almeida, M. *J. Solid State Chem.* **2001**, *159*, 391–402. (g) Min, K. S.; Miller, J. S. *Dalton Trans.* **2006**, 2463–2467. (h) Coronado, E.; Galán-Mascarós, J. R.; Martí-Gastaldo, C. *J. Mater. Chem.* **2006**, *16*, 2685–2689.

(9) (a) Pellaux, R.; Schmalle, H. W.; Huber, R.; Fischer, P.; Hauss, T.; Ouladdiaf, B.; Decurtins, S. *Inorg. Chem.* **1997**, *36*, 2301–2308. (b) Decurtins, S.; Schmalle, H. W.; Schneuwly, P.; Oswald, H. R. *Inorg. Chem.* **1993**, *32*, 1888–1892. (c) Decurtins, S.; Schmalle, H. W.; Schneuwly, P.; Ensling, J.; Gütlich, P. *J. Am. Chem. Soc.* **1994**, *116*, 9521–9528. (d) Hernandez-Molina, M.; Lloret, F.; Ruiz-Pérez, C.; Julve, M. *Inorg. Chem.* **1998**, *37*, 4131–4135. (e) Coronado, E.; Galán-Mascarós, J. R.; Gómez-García, C. J.; Martínez-Agudo, J. M. *Inorg. Chem.* **2001**, *40*, 113–120. (f) Pointillart, F.; Train, C.; Gruselle, M.; Villain, F.; Schmalle, H. W.; Talbot, D.; Gredin, P.; Decurtins, S.; Verdaguer, M. *Chem. Mater.* **2004**, *16*, 832–841. (g) Clemente-León, M.; Coronado, E.; Gómez-García, C. J.; Soriano-Portillo, A. *Inorg. Chem.* **2006**, *45*, 5653–5660.

(10) (a) Ballester, G.; Coronado, E.; Giménez-Saiz, C.; Romero, F. M. *Angew. Chem., Int. Ed.* **2001**, *40*, 792–795.

(11) Coronado, E.; Galán-Mascarós, J. R.; Martí-Gastaldo, C. *J. Am. Chem. Soc.* **2008**, *130*, 14987−14988; *CrystEngComm* **2009**, *11*, 2143−2153.

(12) (a) Coronado, E.; Galán-Mascarós, J. R.; Gómez-García, C. J.; Martí-Gastaldo, C. *Inorg. Chem.* **2005**, *44*, 6197–6202. (b) Coronado, E.; Galán-Mascarós, J. R.; Martí-Gastaldo, C. *Polyhedron* **2007**, *26*, 2101–2104. (c) Coronado, E.; Galán-Mascarós, J. R.; Martí-Gastaldo, C.; Waerenborgh, J. C.; Gaczynski, P. *Inorg. Chem.* **2008**, *47*, 6829–6839.

(13) Coronado, E.; Galán-Mascarós, J. R.; Martí-Gastaldo, C. *Inorg. Chem.* **2007**, *46*, 8108–8110.

(14) (a) Neo, K. E.; Ong, Y. Y.; Huynh, H. V.; Hor, T. S. A. *J. Mater. Chem.* **2007**, *17*, 1002–1006. (b) Boudaren, C.; Auffrédic, J. P.; Louër, M.; Louër., D. *Chem. Mater.* **2000**, *12*, 2324–2333.

(15) (a) Cavallini, M.; Albonetti, C.; Biscarini, F. *Adv. Mater.* **2009**, *21*, 1043–1053. (b) Cavallini, M. *J. Mater. Chem.* **2009**, *19*, 6085–6092. (c) Corradini, V.; Menozzi, C.; Cavallini, M.; Biscarini, F.; Betti, M. G.; Mariani, C. *Surf. Sci.* **2003**, *532*, 249–254. (d) Leclere, P.; Surin, M.; Lazzaroni, R.; Kilbinger, A. F. M.; Henze, O.; Jonkheijm, P.; Biscarini, F.; Cavallini, M.; Feast, W. J.; Meijer, E. W.; Schenning, A. *J. Mater. Chem.* **2004**, *14*, 1959–1963.

(16) (a) Cavallini, M.; Biscarini, F.; Gomez-Segura, J.; Ruiz, D.; Veciana, J. *Nano Lett.* **2003**, *3*, 1527–1530. (b) Leyva, A. G.; Stoliar, P.; Rosenbusch, M.; Lorenzo, V.; Levy, P.; Albonetti, C.; Cavallini, M.; Biscarini, F.; Troiani, H. E.; Curiale, J.; Sanchez, R. D. *J. Solid State Chem.* **2004**, *177*, 3949–3953. (c) Cavallini, M.; Facchini, M.; Albonetti, C.; Biscarini, F. *Phys. Chem. Chem. Phys.* **2008**, *10*, 784–793. (d) Cavallini, M.; Bergenti, I.; Milita, S.; Ruani, G.; Salitros, I.; Qu, Z. R.; Chandrasekar, R.; Ruben, M. *Angew. Chem., Int. Ed.* **2008**, *47*, 8596–8600.

(17) Baylar, J. M.; Jones, E. M. *Inorganic Synthesis*; Booth, H. S., Ed.; McGraw-Hill: New York, 1939.

solid was filtered under vacuum, washed thoroughly with cold water, and dried under vacuum. It was stored in the refrigerator and protected from light to avoid further reduction. The $Tl_3[Fe(ox)_3]$ derivative was prepared by using a previously described synthesis with minor modifications.[18] According to that synthesis, a saturated solution of $[Fe(ox)_3]^{3-}$(aq) was prepared by dissolving its potassium salt (3 mmol; 1.47 g) in the minimum amount of water. Next, a freshly prepared aqueous solution containing an excess of $TlNO_3$ (4.5 mmol; 1.20 g) was added drop by drop. Afterwards, the resulting green solution was protected from light and left to stand overnight. The next morning, the green prismatic crystals that formed were filtered, washed thoroughly with methanol, and dried in air. The product was stored in the refrigerator and protected from light to avoid further reduction.

$\{[Co(H_2O)_2]_3[Cr(ox)_3]_2$(18-crown-6)$_2\}$ (1). Compound **1** was prepared as follows. $Ag_3[Cr(ox)_3]$ (2 mmol; 1.4 g) and $CoCl_2 \cdot 6H_2O$ (3 mmol; 0.72 g) were suspended in 15 mL of methanol and mechanically stirred for 20 min. The resulting AgCl white precipitate was removed by filtration. Next, solid 18-crown-6 (2 mmol; 0.53 g) was added dropwise onto the purple solution and the resulting mixture was stirred. Although the product formation was observed within 15 min, stirring was maintained for a longer period of time. The purple solid was filtered, washed thoroughly with cold methanol, and dried under vacuum. Anal. Calcd for $C_{36}H_{60}Co_3Cr_2O_{42}$ (M_w = 1445.63): C, 29.91; H, 4.18. Found: C, 29.63; H, 4.18. FT-IR: ν[C−H] 2917, 2891, 1461, 1438 cm^{-1}; ν[C═O] 1698, 1662, 1628 cm^{-1}; ν[C−O] 1407, 1353, 1299, 1273 cm^{-1}; ν[C−O] 1104 cm-$^{-1}$; ν[C−C] 959, 912 cm^{-1}; ν[O−C═O] 822, 810 cm^{-1}; ν[M-O] 544, 474, 432, 412 cm^{-1}. Single crystals of **1** suitable for X-ray crystallography were prepared by slow diffusion experiments as described somewhere else.[13]

$\{[Mn(H_2O)_2]_3[Cr(ox)_3]_2$(18-crown-6)$_2\}$ (2). Compound **2** was prepared as for **1**, but using $MnCl_2 \cdot 4H_2O$ (3 mmol; 0.60 g) instead of $CoCl_2 \cdot 6H_2O$. **2** was isolated as a pale purple solid. It was washed thoroughly with cold methanol and dried under vacuum. Anal. Calcd for $C_{36}H_{60}Mn_3Cr_2O_{42}$ (M_w = 1433.65): C, 30.16; H, 4.22. Found: C, 30.04; H, 4.24. FT-IR: ν[C−H] 2915, 2885, 1460, 1434 cm^{-1}; ν[C═O] 1665, 1631 cm^{-1}; ν[C−O] 1398, 1342, 1301 cm^{-1}; ν[C−O] 1108 cm-$^{-1}$; ν[C−C] 907 cm^{-1}; ν[O−C═O] 825, 809 cm^{-1}; ν[M−O] 539, 481, 435, 414 cm^{-1}.

$\{[Mn(H_2O)_2]_{1.5}[Ni(H_2O)_2]_{1.5}[Cr(ox)_3]_2$(18-crown-6)$_2\}$ (3). $Ag_3[Cr(ox)_3]$ (2 mmol; 1.4 g) and $MnCl_2 \cdot 4H_2O$ (1.5 mmol; 0.30 g) were suspended in 15 mL of methanol, and the mixture was mechanically stirred for 20 min. The resulting AgCl white precipitate was removed by filtration. Next, solid $NiCl_2 \cdot 4H_2O$ (1.5 mmol; 0.30 g) was added to the purple solution and the mixture was stirred for 5 min. Once the Ni^{2+} complex was dissolved, 18-crown-6 (2 mmol; 0.53 g) was added dropwise onto the solution and the resulting mixture was stirred for 60 min. The resulting purple solid was filtered, washed thoroughly with cold methanol, and dried under vacuum. Anal. Calcd for $C_{36}H_{60}Mn_{1.5}Ni_{1.5}Cr_2O_{42}$ (M_w = 1439.29): C, 30.04; H, 4.20. Found: C, 29.85; H, 4.14. FT-IR: ν[C−H] 2916, 2891, 2833 1461, 1437 cm^{-1}; ν[C═O] 1698, 1628 cm^{-1}; ν[C−O] 1407, 1354, 1299, 1273, 1255 cm^{-1}; ν[C−O] 1104 cm-$^{-1}$; ν[C−C] 958, 912 cm^{-1}; ν[O−C═O] 821, 810 cm^{-1}; ν[M−O] 544, 474, 430, 412 cm^{-1}.

$\{[Co(H_2O)_2]_{1.5}[Ni(H_2O)_2]_{1.5}[Cr(ox)_3]_2$(18-crown-6)$_2\}$ (4). Compound **4** was prepared as for **3** but using $CoCl_2 \cdot 6H_2O$ (1.5 mmol; 0.36 g) instead of $MnCl_2 \cdot 4H_2O$. **4** was isolated as a pale purple solid. It was washed thoroughly with cold methanol and dried under vacuum. Anal. Calcd for $C_{36}H_{60}Co_{1.5}Ni_{1.5}Cr_2O_{42}$ (M_w = 1445.28): C, 29.92; H, 4.18. Found: C, 30.10; H, 4.22. FT-IR: ν[C−H] 2916, 2891, 1462, 1439 cm^{-1}; ν[C═O] 1699, 1662, 1628 cm^{-1}; ν[C−O] 1407, 1353, 1299, 1255 cm^{-1}; ν[C−O] 1104 cm^{-1}; ν[C−C] 959, 913 cm^{-1}; ν[O−C═O] 821, 811 cm^{-1}; ν[M−O] 545, 473, 433, 413 cm^{-1}.

$\{[Mn(H_2O)_2]_3[Fe(ox)_3]_2$(18-crown-6)$_2\}$ (5). $Tl_3[Fe(ox)_3]$ (2 mmol; 1.90 g) and $MnCl_2 \cdot 4H_2O$ (3 mmol; 0.60 g) were suspended in 15 mL of methanol and mechanically stirred for 20 min. The resulting TlCl white precipitate was removed by filtration. Next, solid 18-crown-6 (2 mmol; 0.53 g) was added dropwise onto the yellowish solution and the resulting mixture was stirred for 60 min. The orange solid that formed was filtered, washed thoroughly with cold methanol, dried under vacuum, and stored protected from light. Anal. Calcd for $C_{36}H_{60}Mn_3Fe_2O_{42}$ (M_w = 1441.35): C, 30.0; H, 4.20. Found: C, 30.10; H, 4.18. FT-IR: ν[C−H] 2911, 1456, 1431 cm^{-1}; ν[C═O] 1694, 1625 cm^{-1}; ν[C−O] 1352, 1303, 1255 cm^{-1}; ν[C−O] 1098 cm-$^{-1}$; ν[C−C] 961, 906 cm^{-1}; ν[O−C═O] 842, 805 cm^{-1}; ν[M−O] 535, 483, 417 cm^{-1}.

$\{[Mn(H_2O)_2]_{1.5}[Co(H_2O)_2]_{1.5}[Fe(ox)_3]_2$(18-crown-6)$_2\}$ (6). $Tl_3[Fe(ox)_3]$ (2 mmol; 1.90 g) and $MnCl_2 \cdot 4H_2O$ (1.5 mmol; 0.30 g) were suspended in 15 mL of methanol, and the mixture was mechanically stirred for 20 min. The resulting TlCl white precipitate was removed by filtration. Next, solid $CoCl_2 \cdot 6H_2O$ (1.5 mmol; 0.36 g) was added to the orange solution and the mixture was stirred for 5 min. Once the Co^{2+} complex was dissolved, 18-crown-6 (2 mmol; 0.53 g) was added dropwise onto the solution and the resulting mixture was stirred for 60 min. The resulting solid exhibited an intense orange color. It was filtered, washed thoroughly with cold methanol, dried under vacuum, and stored protected from light. **6** was isolated as a yellow solid. Anal. Calcd for $C_{36}H_{60}Mn_{1.5}Co_{1.5}Fe_2O_{42}$ (M_w = 1447.34): C, 29.88; H, 4.18. Found: C, 29.7; H, 4.05. FT-IR: ν[C−H] 2908, 2893, 2827, 1455, 1432 cm^{-1}; ν[C═O] 1689, 1627 cm^{-1}; ν[C−O] 1402, 1351, 1304, 1255 cm^{-1}; ν[C−O] 1106 cm-$^{-1}$; ν[C−C] 960, 906 cm^{-1}; ν[O−C═O] 838, 808 cm^{-1}; ν[M-O] 533, 483, 415 cm^{-1}.

$\{[Fe(H_2O)_2]_3[Fe(ox)_3]_2$(18-crown-6)$_2\}$ (7). Compound **7** was prepared as for **5** but using $FeCl_2 \cdot 4H_2O$ (3 mmol; 0.60 g) instead of $MnCl_2 \cdot 4H_2O$. **4** was isolated as a yellowish solid. It was washed thoroughly with cold methanol, dried under vacuum, and stored protected from light. Anal. Calcd for $C_{36}H_{60}Fe_5O_{42}$ (M_w = 1444.07): C, 29.94; H, 4.19. Found: C, 29.73; H, 4.23. FT-IR: ν[C−H] 2907, 1455, 1433 cm^{-1}; ν[C═O] 1694, 1628 cm^{-1}; ν[C−O] 1351, 1300, 1255 cm^{-1}; ν[C−O] 1097 cm-$^{-1}$; ν[C−C] 963, 906 cm^{-1}; ν[O−C═O] 844, 803 cm^{-1}; ν[M−O] 532, 483, 434, 419 cm^{-1}.

$\{[Fe(H_2O)_2]_{1.5}[Ni(H_2O)_2]_{1.5}[Fe(ox)_3]_2$(18-crown-6)$_2\}$ (8). Compound **8** was prepared as for **6** but using $NiCl_2 \cdot 4H_2O$ (1.5 mmol; 0.30 g) instead of $CoCl_2 \cdot 6H_2O$. **8** was isolated as an orange solid. It was washed thoroughly with cold methanol, dried under vacuum, and stored protected from light. Anal. Calcd for $C_{36}H_{60}Ni_{1.5}Fe_{3.5}O_{42}$ (M_w = 1448.34): C, 29.85; H, 4.18. Found: C, 29.73; H, 4.20. FT-IR: ν[C−H] 2910, 2833, 1459, 1435 cm^{-1}; ν[C═O] 1695, 1624 cm^{-1}; ν[C−O] 1400, 1351, 1301, 1255 cm^{-1}; ν[C−O] 1097 cm^{-1}; ν[C−C] 963, 907 cm^{-1}; ν[O−C═O] 842, 806 cm^{-1}; ν[M−O] 535, 483, 424 cm^{-1}.

$Co^{II}_{0.9}Co^{III}_{0.9}Cr^{III}_{1.2}O_4$ (9). **1** was transferred as a finely divided powder into a porcelain crucible and warmed in a muffle furnace up to 450 °C with a 5 °C/min rate. This temperature was maintained an for additional 45 min. Finally, the system was cooled to room temperature with a −10 °C/min rate. **9** was isolated as a black shiny powder, transferred to a vial, and stored under vacuum: $Co_{1.8}Cr_{1.2}O_4$ (M_w = 232.47).

$Mn^{II}_{0.9}Mn^{III}_{0.9}Cr^{III}_{1.2}O_4$ (10). Compound **10** was obtained from **2** by using the same protocol employed for **9**. **10** was isolated as a brownish powder, transferred to a vial, and stored under vacuum: $Mn_{1.8}Cr_{1.2}O_4$ (M_w = 225.28).

$Ni^{II}_{0.9}Mn^{III}_{0.9}Cr^{III}_{1.2}O_4$ (11). Compound **11** was obtained from **3** by using the same protocol employed for **9**. **11** was isolated as a black powder, transferred to a vial, and stored under vacuum: $Mn_{0.9}Ni_{0.9}Cr_{1.2}O_4$ (M_w = 228.66).

$Ni^{II}_{0.9}Co^{III}_{0.9}Cr^{III}_{1.2}O_4$ (12). Compound **12** was obtained from **4** by using the same protocol employed for **9**. **12** was isolated as a black powder, transferred to a vial, and stored under vacuum: $Co_{0.9}Ni_{0.9}Cr_{1.2}O_4$ (M_w = 232.26).

(18) Wyrouboff, G. *Bl. Soc. Min.* **1900**, *23*, 120.

Table 1. Main Structural Parameters of **1** Extracted from Ref 13

formula	$C_{36}H_{60}Co_3Cr_2O_{42}$
M_w	1445.63
space group	$Pc2_1n$
a (Å)	14.395(4)
b (Å)	15.650(5)
c (Å)	26.670(10)
V (Å^3)	6008.3(3)
Z	4
T (K)	293(2)
λ (Å)	0.710 73
ρ_{calcd} (g/cm^3)	1.598
μ (mm^{-1})	1.265
2θ limit (deg)	5.18−45.48
F(000)	7937
R1[a]	0.0615
wR2[b]	0.1497

[a] $R1 = \sum(F_o - F_c)/\sum(F_o)$. [b] $wR2 = [\sum[w(F_o^2 - F_c^2)^2]/\sum[w(F_o^2)^2]]^{1/2}$; $w = 1/[\sigma^2(F_o^2) + (0.0343P)^2 + 2.4502P]$; $P = (F_o^2 + 2F_c^2)/3$.

$(Mn_{0.9}Fe_{0.9})^{II,III}Fe^{III}_{1.2}O_4$ (13). Compound **13** was obtained from **5** by using the same protocol employed for **9**. **13** was isolated as a black powder, transferred to a vial, and stored under vacuum: $Mn_{0.9}Fe_{2.1}O_4$ (M_w = 230.72).

$(Mn_{0.9}Co_{0.9})^{II,III}Fe^{III}_{1.2}O_4$ (14). Compound **14** was obtained from **6** by using the same protocol employed for **9**. **14** was isolated as a reddish powder, transferred to a vial, and stored under vacuum: $Mn_{0.9}Co_{0.9}Fe_{1.2}O_4$ (M_w = 233.50).

Physical Characterization. Metallic Composition. The metallic composition of bulk samples was estimated by electron probe microanalysis (EPMA) performed in a Philips SEM XL30 equipped with an EDAX microprobe. Data concerning compounds **1**−**8** are summarized in Table SI1 (Supporting Information). Oxides have not been included in this study, because they result from the thermal treatment of their molecular precursors.

Elemental Analysis. Carbon, nitrogen, and hydrogen contents of **1**−**8** were determined by microanalytical procedures using an EA 1110 CHNS-O elemental analyzer from CE Instruments.

FT-IR Spectroscopy. Infrared spectra were recorded with a FT-IR Nicolet 5700 spectrometer in the 4000−400 cm^{-1} range using powdered samples diluted in KBr pellets (Table SI2, Supporting Information).

X-ray Single-Crystal Data Collection and Analysis. A dark purple prismatic single crystal of **1** (0.2 × 0.2 × 0.1 mm) was fixed on a glass fiber using crystallographic grease and mounted on a Kappa CCD diffractometer equipped with graphite-monochromated Mo Kα radiation (λ = 0.710 73 Å). Data were collected at 293 K. Cell refinements and data reduction were performed using the Denzo and Scalepack programs.[19] The structure was solved by direct methods using the SIR97 program[20] and refined on F^2 with the SHELXL-97 program.[21] All the non-hydrogen atoms were refined anisotropically. The positions for all the H atoms were calculated, and their thermal parameters were fixed to be 50% larger than those of the atoms to which they are bound. Reference 13 and CCDC 635244 contain the supplementary crystallographic data for **1**. It can be obtained free of charge via www.ccdc.cam.ac.uk/retrieving.html or from the Cambridge Crystallographic Data Center (12 Union Road, Cambridge CB2 1EZ, U.K., fax (+44) 1223-336-033, deposit@ccdc.cam.ac.uk). All crystallographic plots were obtained via the CrystalMaker program.[22] Crystal, data collection, and refinement parameters for **1** are summarized in Table 1.

X-ray Powder Diffraction. X-ray powder profiles of **1**−**8** were collected at 120(4) K with an Oxford Diffraction Gemini A-Ultra X-ray diffractometer equipped with an Enhance Cu source (λ_α = 1.541 84 Å), a 0.5 mm collimator, and a 92 mm diagonal Sapphire CCD detector. Samples were grounded and transferred to a 0.5 mm internal diameter glass capillary. Typically, profiles were collected as step scans over a 15 min period in the 10° < 2θ < 75° range. The theoretical X-ray diffraction pattern for compound **1** was simulated from the atomic coordinates of its crystalline structure by using the CrystalDiffract software package.[22] X-ray diffraction data for compounds **1**−**8** were indexed on an orthorhombic space group and refined using the Unitcell program.[23] X-ray powder profiles of **9**−**14** were collected at 293(2) K with a Bruker-AXS d5005 X-ray diffractometer equipped with 2.2 kW sealed Cu Kα source (λ_α = 1.541 84 Å), diffracted beam monochromator, rotatory sampler, and scintillation counter detector. Samples were grounded and mounted on a flat sample plate. Typically, profiles were collected as step scans over a 12 h period in the 10° < 2θ < 60° range with a step size of 0.02°. Finally, X-ray diffraction patterns were indexed on a cubic space group and refined using the same program.

Magnetic Measurements. Magnetic susceptibility measurements of **2**−**8** and **9**−**14** were performed on powdered samples, whereas magnetic measurements of **1** were performed on both hand-collected ground crystals and a polycrystalline sample. No remarkable difference was observed between them. Magnetic data were collected with a Quantum Design MPMS-XL-5 susceptometer equipped with a SQUID sensor and a Quantum Design PPMS-9 model. The latter was used only for the collection of dynamic magnetic measurements at frequencies higher than 1000 Hz. The susceptibility data were corrected from the diamagnetic contributions of the atomic constituents of the samples, as deduced by using Pascal's constant tables and the samples holder. dc static data were collected in the range 2−300 K with an applied field of 1000 or 100 G (**3**), and hysteresis loops were collected between −5 and +5 T at 2 K. ac dynamic data were collected in the range 2−25 K (**1**−**8**) and 10−300 K (**9**−**14**) with an applied alternating field of 3.95 G at different frequencies in the range 1−10 000 Hz.

Lithographically Controlled Wetting (LCW). The stamp for LWC was a piece of polycarbonate coated with an Al film that was >100 nm thick. The stamp motif is composed of parallel lines with a periodicity of 1.5 μm, a width of 550 nm, and a depth of 230 ± 15 nm.[24] The substrates consist of a 10 × 10 mm^2 piece of silicon (110) covered by ∼2 nm of native silicon oxide. They were cleaned by sonication for 2 min in electronic-grade water (millipure quality), 2 min in acetone (Aldrich chromatographic quality), and 2 min in propanol (Aldrich spectroscopic grade quality). Solutions were prepared using deionized water.

Atomic Force Microscopy (AFM). Images were recorded with a commercial AFM (NT-MDT) operating in air, in intermittent contact mode (25° with relative humidity 55%). Si_3N_4 cantilevers, with typical curvature radius of a tip 10 nm, were employed.

Magnetic Force Microscopy (MFM). Images were collected with a SMENA MFM (NT-MDT) using the lift mode. Magnetic tips were used as commercially supplied (NT-MDT FMG01/Co).

Results and Discussion

Synthesis. A total of 14 compounds were synthesized. They can be divided into two different categories: (a) the family of

(19) Otwinowski, Z.; Minor, W. *Methods in Enzymology*; Carter, C. W., Jr., Sweet, R. M., Eds.; Academic Press: New York, 1997; Vol. 276, pp 307−326.
(20) Altomare, A.; Burla, M. C.; Camali, M.; Cascarano, G. L.; Giacovazzo, C.; Guagliardi, A.; Moliterni, A. G. G.; Polidori, G.; Spagna, R. *J. Appl. Crystallogr.* **1999**, *32*, 115–119.
(21) Sheldrick, G. M. SHELXL-97; University of Göttingen, Göttingen, Germany, 1997.
(22) CrystalMaker; CrystalMaker Software, Oxford, U.K., 2006.
(23) Holland, T. J. B.; Redfern, S. A. T. *Mineral. Magn.* **1997**, *61*, 65.
(24) (a) Cavallini, M.; Gomez-Segura, J.; Albonetti, C.; Ruiz-Molina, D.; Veciana, J.; Biscarini, F. *J. Phys. Chem. B* **2006**, *110*, 11607–11610. (b) Innocenti, M.; Cattarin, S.; Cavallini, M.; Loglio, F.; Foresti, M. L. *J. Electroanal. Chem.* **2002**, *532*, 219–225. (c) Cedeno, C. C.; Seekamp, J.; Kam, A. P.; Hoffmann, T.; Zankovych, S.; Torres, C. M. S.; Menozzi, C.; Cavallini, M.; Murgia, M.; Ruani, G.; Biscarini, F.; Behl, M.; Zentel, R.; Ahopelto, *J. Microelectron. Eng.* **2002**, *61*−*62*, 25–31. (d) Simeone, F. C.; Albonetti, C.; Cavallini, M. *J. Phys. Chem. C* **2009**, *113*, 18987–18994.

Table 2. Unit Cell Constants Refined in an Orthorhombic Space Group for **1**−**8**[a]

	$M^{II}M^{II}M^{III}$	*a* (Å)	*b* (Å)	*c* (Å)	*V* (Å^3)
1[b]	CoCoCr	14.395(4)	15.650(5)	26.670(10)	6008.3(3)
1	CoCoCr	14.2(3)	15.9(4)	27.3(5)	6163(21)
2	MnMnCr	14.3(4)	15.8(4)	26.8(5)	6056(21)
3	MnNiCr	14.3(3)	15.8(4)	27.1(4)	6119(58)
4	CoNiCr	14.1(4)	15.7(3)	27.5(7)	6097(20)
5	MnFeFe	14.4(4)	15.6(5)	26.9(5)	6044(25)
6	MnCoFe	14.4(5)	16.0(4)	26.8(5)	6202(15)
7	FeFeFe	14.6(4)	15.9(3)	27.6(7)	6369(21)
8	FeNiFe	14.5(4)	15.5(3)	27.1(7)	6108(20)

[a] All data refer to bulk samples apart from **1**, which refer to single crystal X-ray diffraction experiments. [b] Cell parameters estimated from X-ray single crystal diffraction extracted from.[13]

Table 3. Lattice Parameters Refined in a Cubic Space Group for **9**−**14**

	formula	*a* (Å)	*V* (Å^3)
9	$Co^{II}_{0.9}Co^{III}_{0.9}Cr^{III}_{1.2}O_4$	8.18(4)	549(8)
10	$Mn^{II}_{0.9}Mn^{III}_{0.9}Cr^{III}_{1.2}O_4$	8.44(4)	601(8)
11	$Ni^{II}_{0.9}Mn^{III}_{0.9}Cr^{III}_{1.2}O_4$	8.31(3)	574(8)
12	$Ni^{II}_{0.9}Co^{III}_{0.9}Cr^{III}_{1.2}O_4$	8.22(4)	555(8)
13	$(Mn_{0.9}Fe_{0.9})^{II,III}Fe^{III}_{1.2}O_4$	8.33(4)	579(8)
14	$(Mn_{0.9}Co_{0.9})^{II,III}Fe^{III}_{1.2}O_4$	8.37(4)	587(8)

layered 2D oxalate-based magnets (**1**−**8**; Table 2) $\{[M^{II}(H_2O)_2]_3[Cr(ox)_3]_2(18\text{-crown-}6)_2\}$ (M^{III} = Cr, Fe; M^{II} = Mn, Fe, Co, Ni), which depending on the nature of the M(III) ion can be further subcategorized into the Cr(III) and Fe(III) series, and (b) the spinel-type intermetallic oxides resulting from their thermal decomposition in air (**9**−**14**; Table 3).

1−**8** were isolated as bulk materials following the same synthetic route: dropwise addition of the neutral 18-crown-6 molecule to a methanolic solution containing the M(II) metallic cations and the corresponding $[M^{III}(ox)_3]^{3-}$ complex. The desired compounds immediately precipitate from solution after the addition of the crown ether moiety. The addition of a cation to the charged components in solution is not necessary for the assembly of the 2D architectures, constituting a remarkable characteristic of these sorts of materials which have only been observed in a recent example reported by Zhang et al.[25] These products are soluble in water, whereas they remain nonsoluble in organic solvents. This chemical property, rarely exhibited by other magnetic CPs,[26] was used to obtain good-quality single crystals of **1**,[13] suitable for X-ray diffraction experiments.

Spinel-type intermetallic oxides (**9**−**14)** were prepared from the thermal decomposition in air of compounds **1**−**6** treated in a muffle furnace up to 450 °C under a controlled heating rate.

Structure. 1 crystallizes in the $Pc2_1n$ orthorhombic space group. It is built by neutral layers of $[Co(H_2O)_2]_3[Cr(ox)_3]_2$. These layers present "holes" that are occupied by the neutral 18-crown-6 guest molecules (Figure 1). These layers are perpendicular to the *ac* plane and are related by an inversion center located in the interlayer space. The absence of an interlamellar cation induces an interlayer distance of 7.825 (2) Å, which is remarkably smaller than those exhibited by the classical cation-templated 2D phases (Table 4). In this "cation-less" phase, each layer is formed by 12-membered rings constituted of six $[Cr(ox)_3]^{3-}$ units and six Co^{2+} atoms. While each chromium atom is shared between three rings, every Co(II) is shared between two neighboring rings. Within these rings, each Co(II) ion is octahedraly coordinated by two bridging bis-bidentate μ_2-oxalate ligands, belonging to two $[Cr(ox)_3]^{3-}$ units, and two water molecules. We can observe two different types of Co^{2+} ions, Co1 and Co2, in a 2:1 ratio. Whereas in Co1 the two water molecules appear in a cis conformation, in Co2 they are bonded in a trans fashion. Each $[Cr(ox)_3]^{3-}$ binds two Co2 and one Co1 center. In the 12-membered rings the metallic centers exhibit alternating chirality with a repeating pattern ...Co2ΛΔΔΛΔΔCo2..., with nonchiral Co2 ions connecting two Cr^{3+} atoms with opposite chirality. Both Co^{2+} centers adopt regular octahedral coordination, with $Co-O_{ox}$ and $Co-O_w$ distances between 2.094(2) and 2.149(2) and between 2.030 and 2.084(2) Å, respectively. The bonding angles slightly deviate from regular octahedral geometry due to the bite angle of the oxalate ligands ($O_{ox}-Co-O_{ox}$ between 78.097 and 79.879°). The local distortion observed in the Cr atom coordination sphere is less intense than that for the Co atoms, with shorter $Cr-O_{ox}$ distance values (between 1.957 and 2.017(2) Å) and less acute angles for the oxalate bridge ($O_{ox}-Cr-O_{ox}$ in the 81.227−82.730° range). Hydrogen-bonding interactions play a key role in the formation of this sort of compound (Figure 2). The two crown ether molecules located in the middle of each 12-membered structural unit are interacting through their oxygen atoms with the bonded water molecules. While the $O_w\cdots O_{Crown}$ distances for the water molecules coordinated in a cis fashion are in the 2.672(2)−3.049(2) Å range, they range between 2.780(2) and 2.989(2) Å for the trans molecules. Most relevant hydrogen-bonding distances for compound **1** are summarized in Table SI3 (Supporting Information). These values are in good agreement with previously reported hydrogen-bonding interactions between coordinated water molecules and crown ether oxygen atoms.[27]

1 was additionally obtained as a polycrystalline powder together with **2**−**8.** All of them were structurally characterized by powder X-ray diffraction. All compounds seem to be isostructural, exhibiting quite analogous diffraction patterns to that simulated from the atomic positional parameters of **1** (Figure SI4, Supporting Information).[13] Cell parameters were obtained from the indexation of the most intense reflections in an orthorhombic crystalline system (Table 2).

Figure SI5 (Supporting Information) shows the X-ray diffraction pattern of mixed oxides **9**−**14**, as resulting from the thermal decomposition of the oxalate-based precursors. They exhibit the typical diffraction pattern for spinel-type oxides with a low-intensity secondary diffraction peak centered on 35.5°. This peak suggests the formation of a residual amount of a contaminant oxide phase together with the spinels during the thermal treatment. The unit cell parameters obtained from the indexation of the main reflections in a cubic space group are summarized in Table 3. All of them are within the range of lattice constants typically attributed to spinel-like oxides containing transition-metal ions. Note that the (311) peak is slightly shifted, depending on the nature of the metallic ions composing the oxide. This fact has previously been observed and attributed to the different ionic radii: larger ions yield larger cell parameters, and accordingly the peak is shifted to smaller

(25) Zhang, B.; Zhang, Y.; Zhang, J.; Lia, J.; Zhu, D. *Dalton Trans.* **2008**, 5037.

(26) (a) Bellito, C.; Day, P. *J. Chem. Soc., Chem. Commun.* **1976**, 870–871. (b) Stead, M. J.; Day, P. *J. Chem. Soc., Dalton Trans.* **1982**, 1081–1084. (c) Kou, H.-Z.; Gao, S.; Li, C.-H.; Liao, D.-Z.; Zhou, B.-C.; Wang, R.-J.; Li, Y. *Inorg. Chem.* **2002**, *41*, 4756–4762.

(27) (a) Rogers, R. D.; Kurihara, L. K.; Benning, M. M. *J. Chem. Soc., Dalton Trans.* **1988**, *1*, 13–16. (b) Steed, J. W.; Junk, P. C. *J. Chem. Soc., Dalton Trans.* **1999**, *13*, 2141–2146.

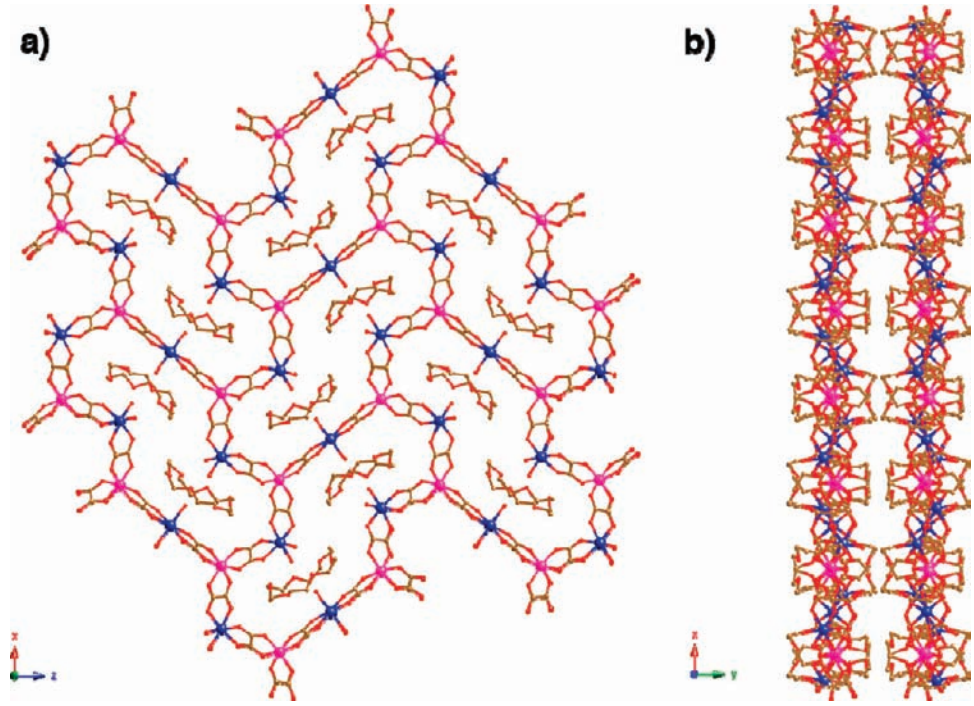

Figure 1. Perspective showing (a) the structure of the neutral polymeric layers of **1** and (b) the packing of these layers along the *b* axis: Cr, pink; Co, blue; O, red; C, black. Hydrogen atoms have been omitted for the sake of simplicity.

Table 4. Interlayer Distances of Several Cation-Templated 2D Oxalate-Based Magnets[a]

cation	2D network	d_{inter} (Å)	no. of peaks fitted	ref
$N(n\text{-}C_3H_7)_4$	$Mn^{II}Fe^{III}$	8.19	16	8e
$N(n\text{-}C_4H_9)_4$	$Mn^{II}Cr^{III}$	8.93	singlecrystal	42
$P(n\text{-}C_4H_9)_4$	$Mn^{II}Fe^{III}$	9.20	11	8e
$Fe^{III}Cp^*_2$	$Mn^{II}Cr^{III}$	9.28	singlecrystal	43
$N(C_6H_5CH_2)(n\text{-}C_4H_9)_3$	$Mn^{II}Fe^{III}$	9.43	12	8e
$P(C_6H_5)_4$	$Mn^{II}Cr^{III}$	9.55	singlecrystal	44
$As(C_6H_5)_4$	$Mn^{II}Fe^{III}$	9.57	9	8e
$N(n\text{-}C_5H_{11})_4$	$Mn^{II}Fe^{III}$	10.16	11	8e
$(C_6H_5)_3PNP(C_6H_5)_3$	$Mn^{II}Fe^{III}$	14.52	13	8e

[a] Note that some distances have been extracted from single-crystal X-ray data, whereas others have been estimated from least-squares fitting of the powder diffraction data.

diffraction angles.[28] Spinels are composed of oxide anions arranged in a cubic close-packed lattice and metallic cations, which can be divalent or trivalent, occupying some or all of the octahedral (O_h) and tetrahedral (T_d) vacant positions in the lattice. In the "normal spinel" structure, M^{II} cations occupy the tetrahedral sites of the oxide lattice and M^{III} cations the octahedral sites. For inverse spinels, half the M^{III} cations occupy the tetrahedral sites, and both M^{II} and M^{III} cations occupy the octahedral sites. According to experimental reports, depending on the synthetic protocol employed, partial inversion of the spinel structure can occur in some cases.[29] Given that the T_d and O_h sites in the lattice generate different crystal field stabilization energies, crystal field theory has been widely invoked to explain the distribution of the cations within the spinels.[30] Nevertheless, in many cases the energy difference between the different cationic sites is minimum and does not allow for an accurate determination of the position of the cations in the lattice. In addition, the redox versatility exhibited by most of the atoms composing these oxides would require additional characterization to find out which are the oxidation states of each metallic atom in these compounds. The determination of the exact distribution of transition-metal ions in the structures of **9**−**14** is therefore a difficult task, which remains beyond the scope of this work.

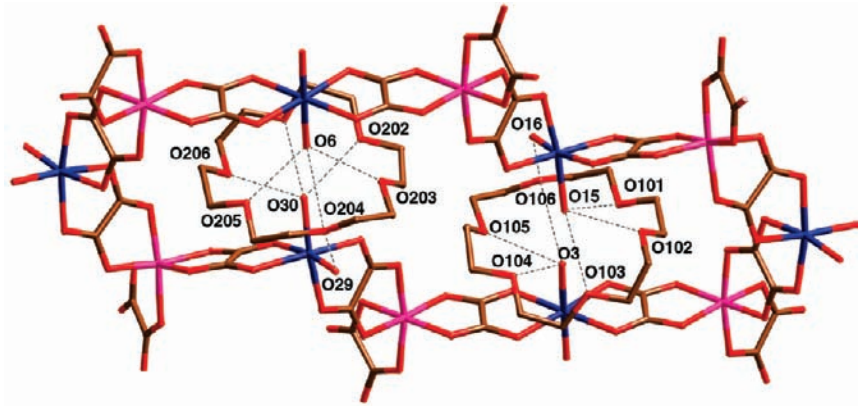

Figure 2. Hydrogen-bonding interactions (dashed bonds) between the 2D oxalate-based framework and the crown ether molecules located in the holes. Hydrogen atoms have been omitted for the sake of simplicity.

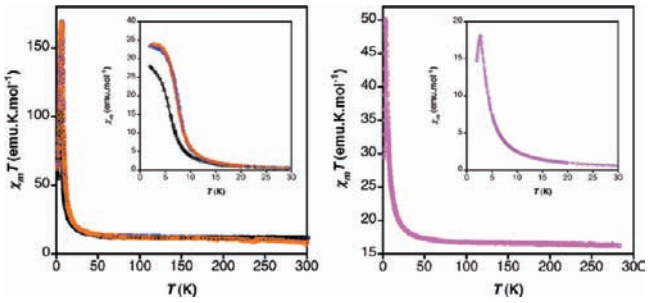

Figure 3. Thermal dependence of the $\chi_M T$ product of **1** (blue), **3** (black), and **4** (orange) measured with an applied field of 1000 G (left) and $\chi_M T$ product of **2** (purple) under an applied field of 1000 G (right). The inset shows the χ_M *vs* T plot in the low-temperature region. Solid lines are only a guide to the eye.

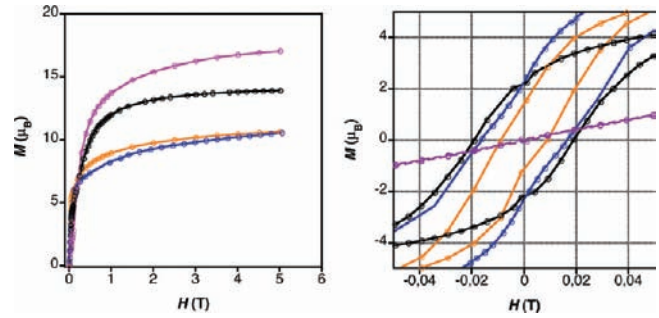

Figure 4. Field dependence of the magnetization (left) and zoom-in of the hysteresis loops focusing on the low-field areas (right) of **1** (blue), **2** (purple), **3** (black), and **4** (orange) measured at 2 K.

Magnetic Properties. (a) Cr^{III} Series. Magnetic susceptibility measurements for **1**−**4** derivatives present almost a constant value for the $\chi_M T$ product value as the temperature decreases down to 20 K (Figure 3). The magnetic susceptibility data can be fitted to a Curie−Weiss law in the high-temperature regime (150−300 K), giving Curie constant values (C) in good agreement with the expected spin-only values (see Table 5 and Figures SI6 and SI7 (Supporting Information)). All compounds present a positive Θ value in the paramagnetic regime, suggesting the presence of ferromagnetic interactions. This fact is in good agreement with the expected superexchange between Cr^{3+} in an octahedral coordination ($S = {}^3/_2$; $t_{2g}{}^3$ electronic configuration) and the neighboring divalent ions through a bis-bidentate chelating oxalate linker. Below 20 K, the $\chi_M T$ product starts to increase and defines a maximum, which corresponds to a steep jump in the χ_M vs T plot, suggesting the onset of a ferromagnetically ordered state. After this jump, χ_M tends to saturation in **1**, **3**, and **4**, whereas it defines a maximum in **2**. This feature commonly suggests the occurrence of antiferromagnetic interactions and must be attributed to the presence of a low percentage of a contaminant phase. In this context, it is worth noting that the synthesis of this family of layered compounds is rather similar to that employed in the isolation of the related compound $\{[Mn(OH_2)(CH_3OH)][Mn(OH_2)_2]_2$-$[Cr(ox)_3]_2(18\text{-crown-}6)\}\cdot CH_3OH$.[31] In that particular case, the presence of a fraction of oxalate ligands acting simultaneously as a bidentate−monodentate bridging ligand promoted the presence of an overall antiferromagnetic interaction between Mn^{2+} and Cr^{3+} ions. Since the composition of **2** is equivalent to that exhibited by this $Mn^{II}Cr^{III}$ oxalate-based ferrimagnet, its magnetic behavior is likely to result from the contribution of the expected ferromagnetic phase with a minor contribution associated to a contaminant ferrimagnetic phase.

The isothermal field dependence of the magnetization confirms the ferromagetic nature of these systems (Figure 4). From low fields, the magnetization increases very rapidly, as expected for the overall ferromagnetic coupling, reaching saturation values slightly smaller than those expected for the parallel alignment of the interacting spins. This deviation has been previously observed for other molecule-based magnets and attributed to the presence of spin canting in the ordered ferromagnetic state.[8a]

To confirm the existence of magnetic ordering and define more precisely the critical ordering temperatures, ac magnetic measurements were performed (Figure 5). All the compounds present a maximum in both the in-phase (χ'_M) and out-of-phase signals (χ''_M). We have considered the critical temperature (T_c) for these systems as the higher temperature for which the out-of-phase signal is nonzero. In this way, critical temperatures range from 7.6 K for **1** down to 3.6 K for **2**. Compounds **1**, **3**, and **4** show sharp, well-defined nonfrequency dependent peaks for both the in-phase and out-of-phase signals. In contrast, **2** shows broader signals and significant dependence of the intensity of the χ_M'' signal with the frequency. This anomalous behavior, in comparison with the rest of the derivatives, must be probably attributed to the residual presence of a contaminant phase (vide supra).

All compounds present hysteresis loops at 2 K and, in view of their coercive fields, can be classified as soft magnets (Figure 4 and Figure SI9 (Supporting Information)). The highest coercive field of 0.16 kG is observed for **1**, probably a result of the presence of highly anisotropic octahedral Co(II) ions.

(b) Fe^{III} Series. Magnetic susceptibility measurements for the **5**−**8** derivatives were performed on powdered samples. All compounds present a decrease in the $\chi_M T$ product values as the systems are cooled. For **5**, **6**, and **8**, $\chi_M T$ clearly defines a minimum at low temperatures that is a typical feature of antiferromagnetic interactions (Figure 6). Susceptibility data in the high-temperature regime (150−300 K) have been fitted to a Curie−Weiss law, yielding Curie constant values (C) in good agreement with the expected spin-only values (Table 5 and

Table 5. Main Magnetic Parameters for **1**−**8**[a]

	$M^{II}M^{II}M^{III}$	χT_{rt}	C	C_{SO}	Θ (K)	T_C (K)	M_S (μ_B)	M_R (μ_B)	H_{Coer} (kG)
1	CoCoCr	11.8	10.9	9.38	22.6	7.6	10.8	2.3	0.16
2	MnMnCr	16.4	16.0	16.88	6.6	3.6	17.0	<0.1	<0.10
3	MnNiCr	12.1	11.9	11.81	2.1	6.8	13.9	2.4	0.20
4	CoNiCr	8.7	8.2	8.06	44.4	6.8	10.7	1.4	0.20
5	MnFeFe	17.5	19.9	21.86	−32.3	19.5	4.8	<0.1	<0.10
6	MnCoFe	17.2	21.7	18.13	−75.6	9.4	2.3	0.3	6.30
7	FeFeFe	14.7	17.1	17.75	−52.2	12.2	1.3	<0.1	1.10
8	FeNiFe	12.6	15.2	14.75	−67.2	20.0	2.7	0.1	0.16

[a] Definitiions: Curie constant, C (emu K mol^{-1}); Curie constant spin-only value, C_{SO} (emu K mol^{-1}); Weiss constant, Θ; critical temperature, T_c; saturation magnetization, M_S; remnant magnetization at 2 K, M_R; coercive field at 2 K, H_{Coer}. $S(Cr^{3+}) = {}^3/_2$, $S(Fe^{3+}) = {}^5/_2$, $S(Mn^{2+}) = {}^5/_2$, $S(Fe^{2+}) = 2$, $S(Co^{2+}) = {}^3/_2$, $S(Ni^{2+}) = 1$.

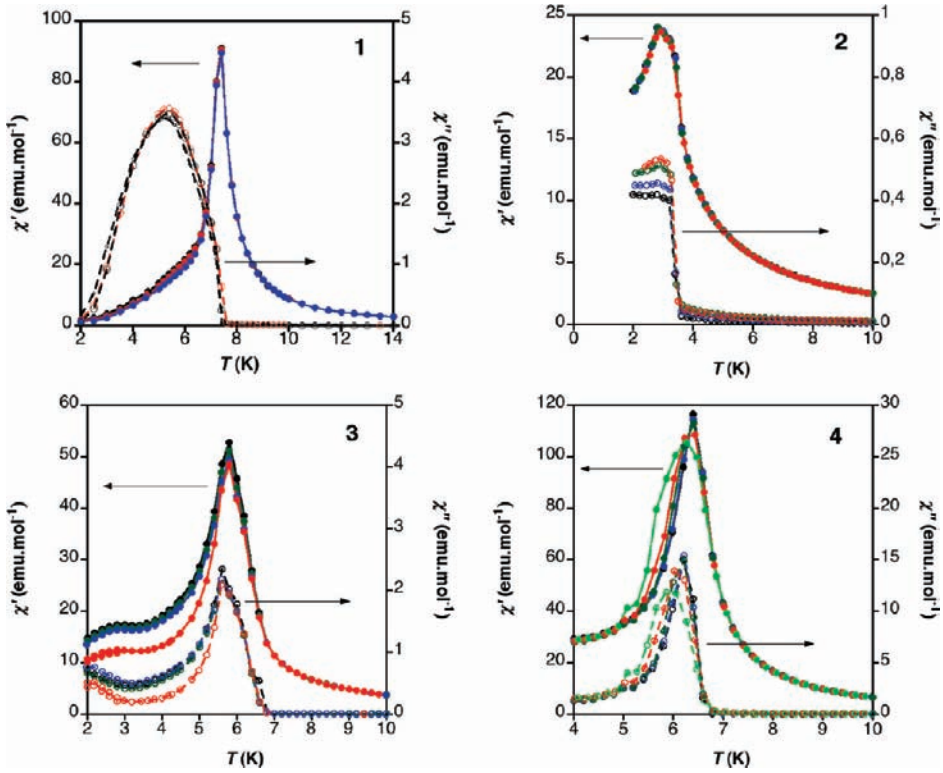

Figure 5. ac susceptibility in the 1−10 000 Hz region of **1**−**4**. In-phase susceptibility is represented by solid symbols, whereas out-of-phase susceptibility is represented by open symbols. Solid lines are only a guide to the eye.

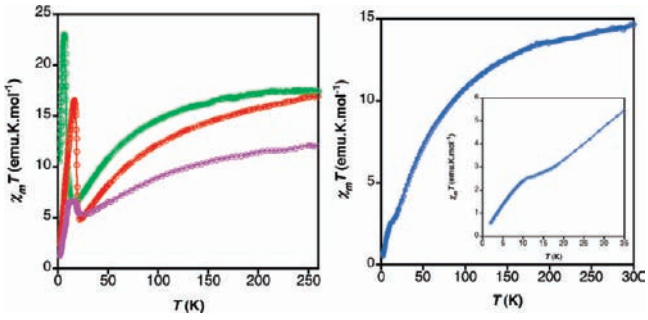

Figure 6. Thermal dependence of the $\chi_M T$ product for **5** (green), **6** (red), **7** (blue; on the right), and **8** (purple). The inset of the figure on the right shows a zoom-in of the $\chi_M T$ product for **7** in the 2−35 K interval. Solid lines are only a guide to the eye.

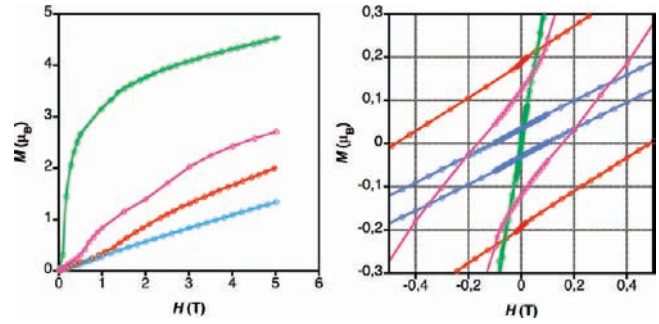

Figure 7. Field dependence of the magnetization (left) and zoom-in of the hysteresis loops highlighting the low-field area (right) of **5** (green), **6** (red), **7** (blue), and **8** (purple) measured at 2 K.

Figure SI8 (Supporting Information)). The large negative values of the Weiss constants (Θ) are indicative of the presence of antiferromagnetic interactions between neighboring metallic centers in all the cases, as expected for the superexchange mediated by the oxalate ligand acting in its bis-bidentate chelating form between octahedrally coordinated Fe^{3+} ($S = {}^5/_2$; $t_{2g}{}^3e_g{}^2$ electronic configuration) and divalent metallic ions. Below 25 K, the $\chi_M T$ product presents an increase in the magnetization, reaching a maximum that corresponds to a steep jump in the χ_M vs T plot, suggesting the onset of long-range magnetic ordering in these systems from antiferromagnetic interactions between noncompensating spins (Figure SI8; $S(Mn^{2+}) = {}^5/_2$, $S(Fe^{2+}) = 2$, $S(Co^{2+}) = {}^3/2$, $S(Ni^{2+}) = 1$).

Figure 7 shows the field dependence of the magnetization of **5**−**8** at 2 K, studied to confirm the nature of the magnetic ordering in these systems. All the compounds, except for **5**, present a linear increase of the magnetization with the applied field, reaching small magnetization values at 5 T. Since the values of the magnetization at high fields are still far from saturation, these compounds can be classified as ferrimagnets. In contrast with the rest of the Fe(III) derivatives, the anomalous rapid increase of the magnetization with the applied field (up to 3.5 μ_B) observed for **5** is probably induced by the softness of the Mn^{2+} ion in an octahedral environment. Finally, we wish to remark that the particular metal stoichiometry exhibited by this family of magnets, M(II):M(III) = 3:2, causes the $Mn^{II}Mn^{II}Fe^{III}$ derivative to behave as a ferrimagnet, whereas weak ferromagnetism is observed in the related $Mn^{II}Fe^{III}$ M(II):M(III) = 1:1 2D layered magnets with honeycomb-like architectures.[8a,e,43]

ac magnetic susceptibility measurements confirm the occurrence of long-range magnetic ordering and allow for an accurate estimation of the ordering temperatures (Figure 8). They range from 20.0 K for **8** down to 9.4 K for **6**. All compounds present well-defined sharp peaks for both the in-phase and out-of-phase signals. In addition, **5** and **8** exhibit a secondary contribution at lower temperatures that might be related to the movement of the domain walls in the ordered ferrimagnetic state. Similar features have been already observed in other molecule-based

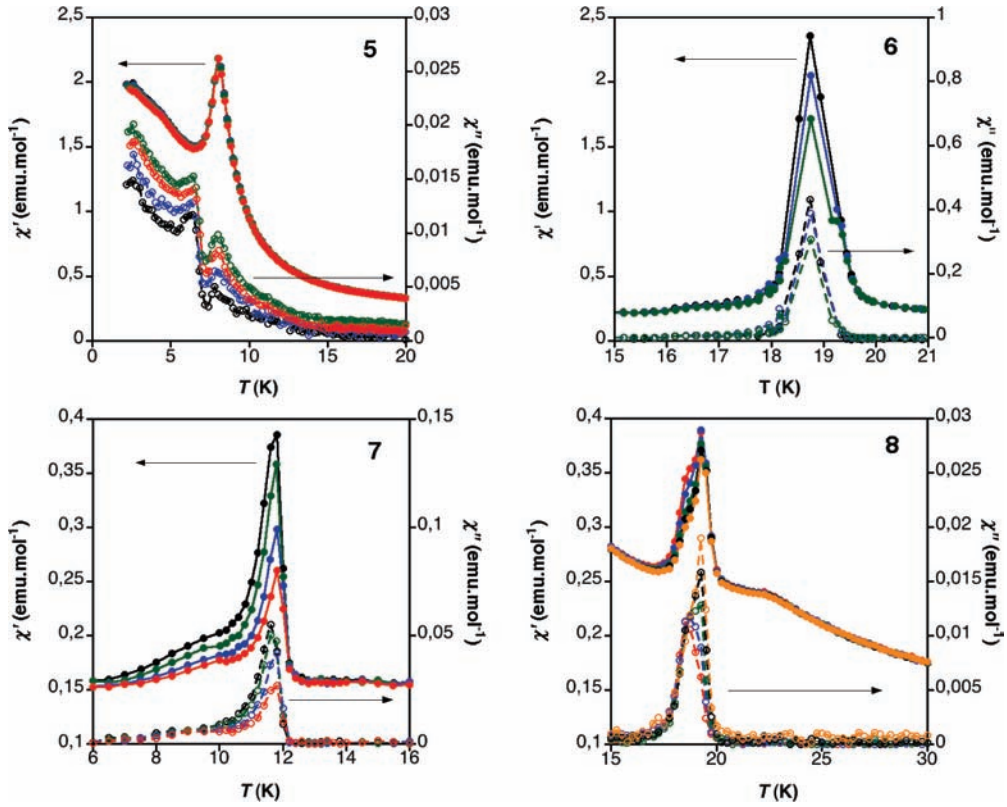

Figure 8. ac susceptibility in the 1−1000 Hz of **5**−**8**. In-phase susceptibility is represented by solid symbols, whereas out-of-phase susceptibility is represented by open symbols. Solid lines are only a guide to the eye.

magnets.[32] Note that minor dependence of the intensity of χ_M' and χ_M'' signals on the frequency in the interval explored (between 1 and 1000 Hz) is observed. This fact must be probably related to the small particle size of the powdered samples employed in the measurements.

Hysteresis loops at 2 K were observed for all the compounds (Figure SI9). Except for **6**, which exhibits the highest coercive field of the series, 6.3 kG, the rest of the compounds can be classified as soft ferrimagnets. As previously pointed out, this fact must be somehow related to the greater anisotropy of octahedral Co^{2+} ions, which introduces greater hardness to the resulting magnetic material.

(c) Spinel-like Oxides. Static and dynamic magnetic measurements were performed on powdered samples of **9**−**14**, as obtained from the thermal decomposition of their oxalate-based molecular precursors. These systems are composed of oxide anions arranged in a cubic close-packed lattice and metallic cations, which can be divalent or trivalent, occupying some or all the octahedral (O_h) and tetrahedral (T_d) vacant positions in the lattice. From a magnetic point of view, this distribution will result in many different magnetic exchange pathways that will depend on the position and the electronic configuration of each paramagnetic center in the lattice. As previously described in the Structure section (vide supra), the accurate estimation of the positions occupied by each metallic atom in the lattice is not an easy task and prevents an extensive magnetic analysis. Moreover, though we extensively surveyed the literature to compare the magnetic behavior of the systems here described with analogous spinel-like oxides prepared through different synthetic routes, we could not extract any remarkable conclusion, given that, even in those cases exhibiting equivalent composition, the constitutional disorder of cations in the lattice is responsible for important deviations in the critical temperature values.[33]

ac susceptibility measurements were performed to check the occurrence of long-range magnetic ordering and determine the critical temperatures at which the onset of magnetic ordering occurred (Figure 9). All compounds present broad peaks for χ_M' and χ_M'' signals in the interval of frequencies explored (1−10 000 Hz). T_c oscillates between 35 K for **13** and room temperature for **14** (Table 6). Neither the χ_M' peaks nor the χ_M'' peaks show any remarkable shift with frequency, typically attributed to glassy-like behavior.[34] Nevertheless, the intensity of the in-phase signal shows strong dependence in some cases. This feature has been previously observed in this work and attributed to the small particle size of the powdered samples measured. Note that the critical temperatures exhibited by these compounds are much greater than those exhibited by **1**−**9**. Magnetic superexchange in **9**−**14** is mediated trough monoatomic oxide anions, whereas the oxalate ligand transports the magnetic moment in **1**−**8**. The reduction of the distance between

(28) (a) Kim, C. K.; Lee, J. H.; Katoh, S.; Murakami, R.; Yoshimura, M. *Mater. Res. Bull.* **2001**, *36*, 2241–2250. (b) Gao, J.; Cui, Y.; Yang, Z. *Mater. Sci. Eng., B* **2004**, *110*, 111–114.
(29) Kamiyama, T.; Haneda, K.; Sato, T.; Ikeda, S.; Asano, H. *Solid State Commun.* **1992**, *81*, 563–566.
(30) Grimes, R. W.; Anderson, A. B.; Heuer, A. H. *J. Am. Chem. Soc.* **1989**, *111*, 1–6.
(31) Coronado, E.; Galán-Mascarós, J. R.; Matí-Gastaldo, C. *Inorg. Chim. Acta* **2008**, *361*, 4017–4023.
(32) Thétiot, F.; Triki, S.; Sala-Pala, J.; Gómez-García, C. J.; Golhen, S. *Chem. Commun.* **2002**, 1078–1079.
(33) Krupicka, S.; Novak, P. In *Oxide Spinels in Ferromagnetic Materials*; Wolfhart, E. P., Ed.; North Holland: Amsterdam, 1982; Vol. 3.
(34) Mydosh, J. A. *Spin Glasses: An Experimental Introduction*; Taylor & Francis: London, 1993.

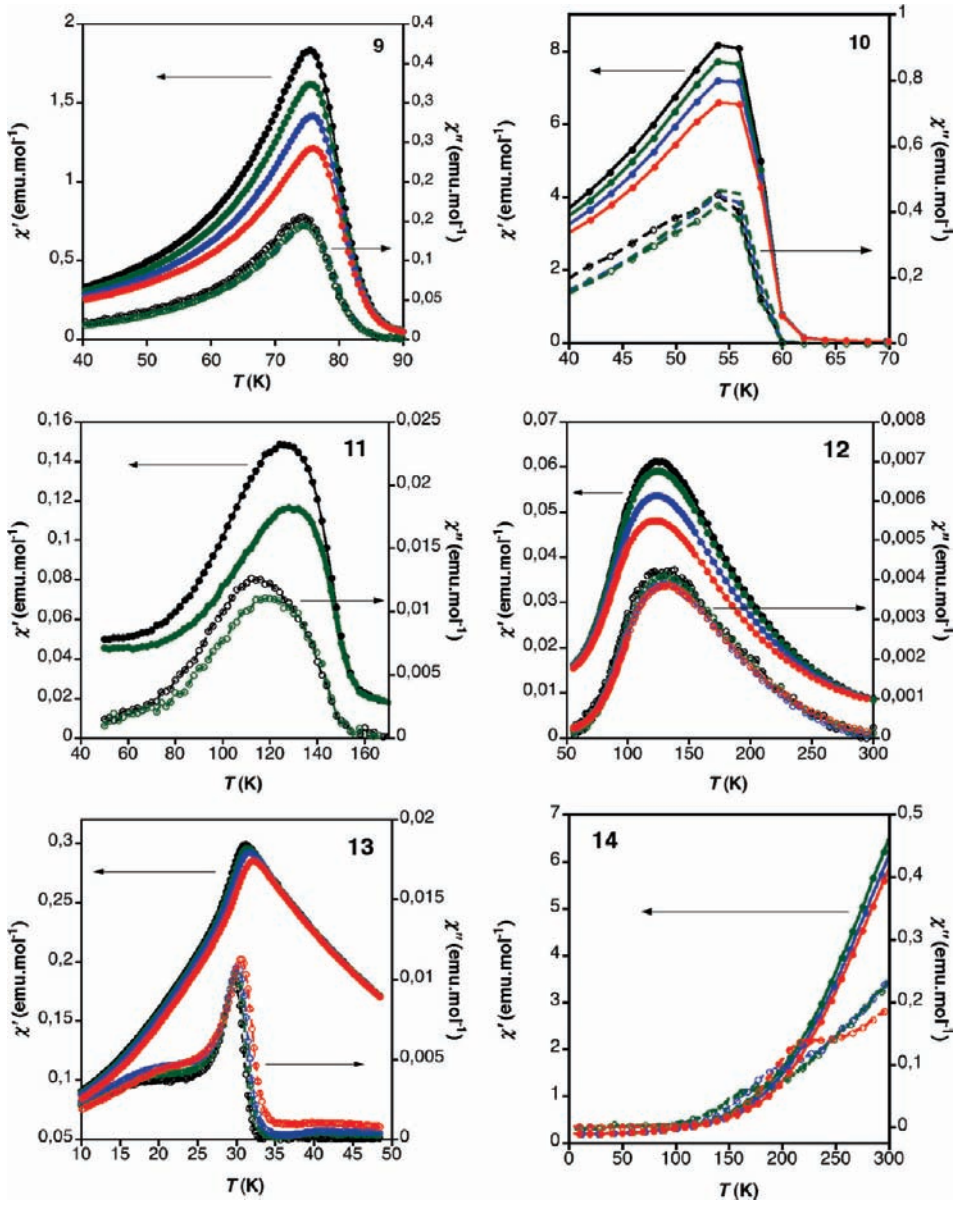

Figure 9. ac susceptibility at 1 (black), 100 (green), 1000 (blue), and 10 000 Hz (red) for **9**−**14**. In-phase susceptibility is represented by solid symbols, whereas out-of-phase susceptibility is represented by open symbols. Solid lines are only a guide to the eye.

Table 6. Main Magnetic Parameters for Compounds **9**−**14**

	formula	χT_{rt}	C	Θ (K)	T_C (K)	M_S (μ_B)	M_R (μ_B)	H_{Coer} (kG)
9	$Co^{II}_{0.9}Co^{III}_{0.9}Cr^{III}_{1.2}O_4$	1.86	2.0	−21.6	86	0.49	0.27	4.5
10	$Mn^{II}_{0.9}Mn^{III}_{0.9}Cr^{III}_{1.2}O_4$	4.03	4.46	−132.5	60	0.92	0.61	1.5
11	$Ni^{II}_{0.9}Mn^{III}_{0.9}Cr^{III}_{1.2}O_4$	2.73	2.75	−103.7	156	0.47	0.17	0.5
12	$Ni^{II}_{0.9}Co^{III}_{0.9}Cr^{III}_{1.2}O_4$	1.60	1.13	108.9	290	0.13	0.02	5.5
13	$(Mn_{0.9}Fe_{0.9})^{II,III}Fe^{III}_{1.2}O_4$	6.16	7.23	−104.4	35	0.86	0.13	3.1
14	$(Mn_{0.9}Co_{0.9})^{II,III}Fe^{III}_{1.2}O_4$	>rt	>rt	>rt	>300?	3.31	2.69	7.1

[a] Definitions: Curie constant, C (emu K mol^{-1}); Curie constant spin-only value, C_{SO} (emu K mol^{-1}), Weiss constant, Θ; critical temperature, T_c; saturation magnetization, M_S; remnant magnetization at 2 K, M_R; coercive field at 2 K, H_{Coer}. $S(Cr^{3+}) = {}^3/_2$, $S(Fe^{3+}) = {}^5/_2$, $S(Mn^{2+}) = {}^5/_2$, $S(Fe^{2+}) = 2$, $S(Co^{2+}) = {}^3/_2$, $S(Ni^{2+}) = 1$.

metallic centers results in a drastic increase of the strength of the magnetic exchange and consequently in an increment of the critical temperature.

Figure 10 shows the field dependence of the magnetization measured at 2 K. Compounds **11**−**13** present a linear increase of the magnetization with the applied field, reaching magnetization values at 5 T (0.47, 0.13, and 0.86 μ_B) very far from saturation. **9**, **10**, and **14** present a greater increase of the magnetization at low fields than their counterparts. After that, magnetization increases linearly with the external applied field and reaches values that are greater than those exhibited by their counterparts (0.49, 0.92, and 3.31 μ_B) but also remain far from saturation. In view of these data, we can conclude that these compounds exhibit ferrimagnetic ordering as result of the overall antiferromagnetic interactions between nonequivalent spins.

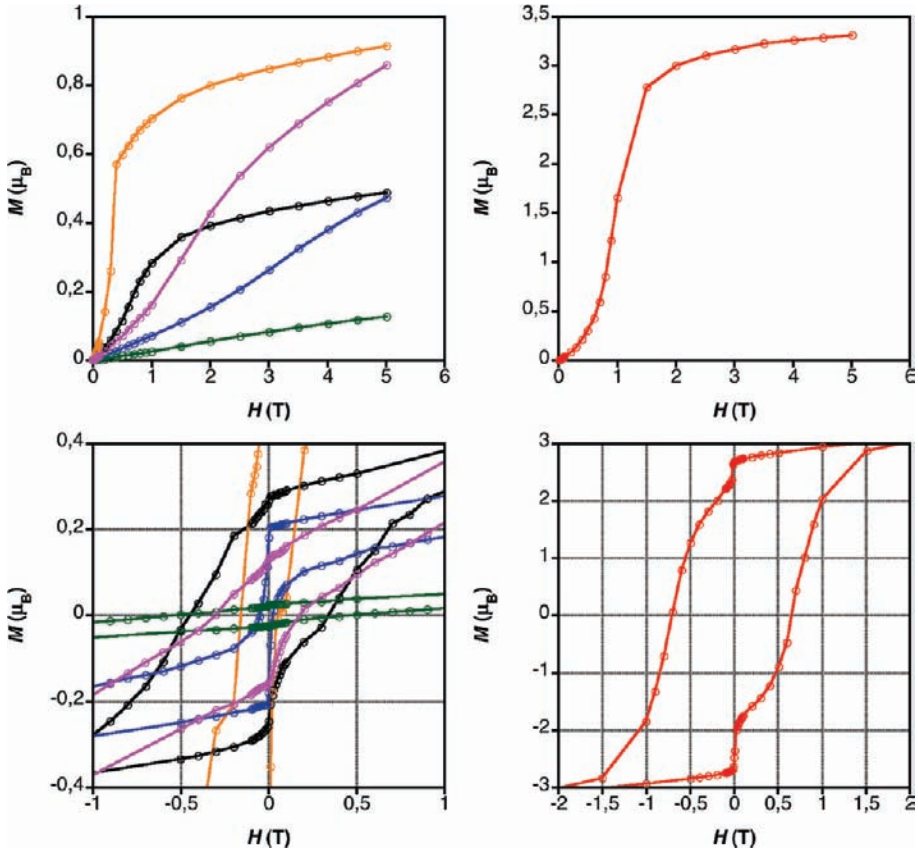

Figure 10. (top) Field dependence of the magnetization measured at 2 K of **9** (black), **10** (orange), **11** (blue), **12** (green), and **13** (purple) on the left and **14** (red) on the right. (bottom) Zoom-in of the hysteresis loops at low fields of **9**−**13** (left) and **14** (right). Solid lines are only a guide to the eye.

Hysteresis loops at 2 K were observed for all the compounds (Figure 10). Remarkable attention must be paid to **14**, presenting the highest coercive field and remnant magnetization, 2.69 μ_B and 7.1 kG, respectively. Compounds **9**, **12**, and **13** can be also classified as hard ferrimagnets, with H_c values in the 5.5−3.1 kG interval, whereas **10** and **11** are softer magnets with H_c values <1.5 kG.

Patterning of Soluble Magnets onto Si(110). Due to their solubility in water, compounds **1**−**8** can be patterned onto solid substrates via unconventional lithography methods.[35] As a proof of concept, here we report the patterning of **6** onto a silicon substrate by means of lithographically controlled wetting (LCW).[36,37]

A schematic representation of the LCW process is represented in Figure 11. In a first step, a droplet of the solution containing the material is spread on a substrate until a thin liquid film is obtained (Figure 11.1). Then, the stamp is gently positioned onto the liquid layer (Figure 11.2). Surface tension keeps the stamp above the fluid and prevents its penetration through it. Afterward, during the solvent evaporation, the volume of the solution becomes comparable to that included between the stamp's protrusions and the substrate so that capillary forces drive the solution to form menisci under the protrusions instead of filling the cavities of the stamp (Figure 11.3). As a result, columns of liquid are formed under the protrusions. As evaporation continues, the saturation limit is reached and the solute precipitates, giving rise to an organized pattern that reproduces the motif of the stamp (Figure 11.4).

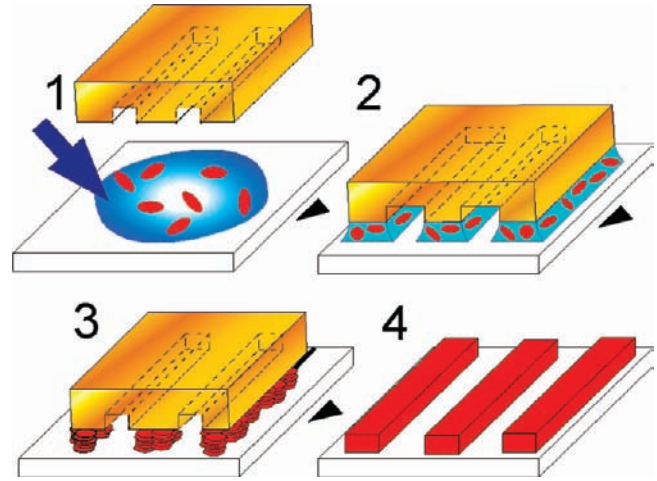

Figure 11. Schematic representation of the LCW method.

In principle this procedure can be generally applied to any soluble material. However, its efficacy depends on several experimental requirements: stamp specifications (material, distance from the substrate, profile, hardness), the solution (solute, solvent, viscosity, density), and the substrate (material, roughness).

Among the oxalate-based precursors, **6** was the most appealing candidate, since the spinel-like oxide resulting from its thermal decomposition behaves as a magnet at room temperature. The result of the deposition of a dilute solution of **6** onto Si(100) is shown in Figure 12. The patterning is effective across a millimeter scale. Notice that this measurement was limited by the maximum scan length of the atomic force microscope

(35) Xia, Y.; Whitesides, G. M. *Angew. Chem., Int. Ed.* **1998**, *37*, 551–575.
(36) Cavallini, M.; Biscarini, F. *Nano Lett.* **2003**, *3*, 1269–1271.

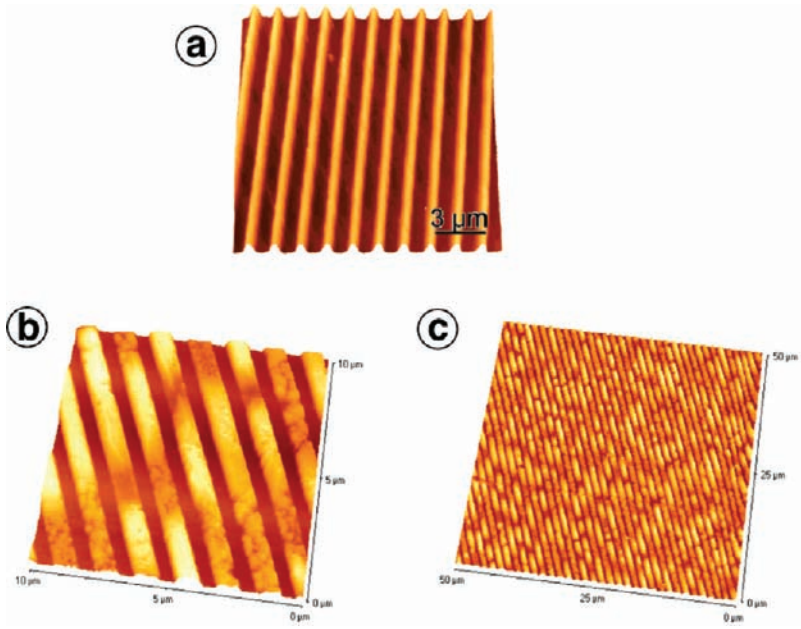

Figure 12. (a) AFM image of the stamp employed in this work. (b) 10 × 10 μm^2 AFM image of the printed lines resulting from the deposition of an aqueous solution of **6** onto Si(110). (c) 50 × 50 μm^2 image.

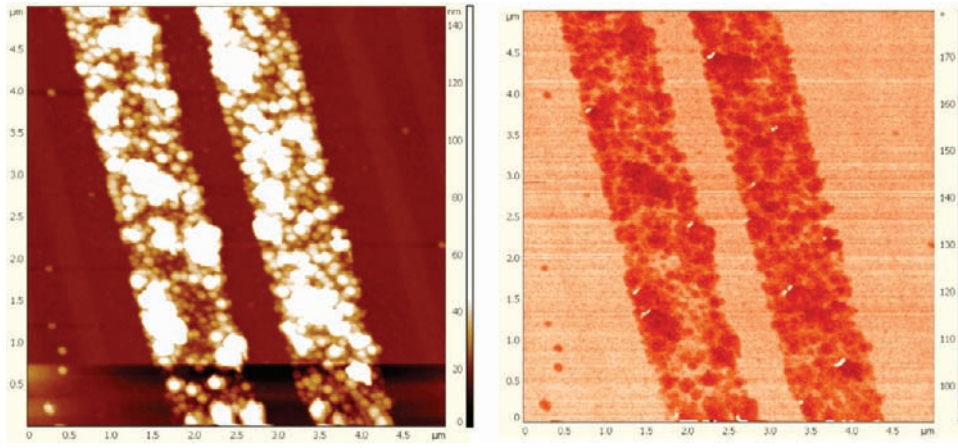

Figure 13. 5 × 5 μm^2 MFM topographic (left) and phase (right) images of the printed pattern after thermal treatment. Images were collected with a lift height of 40 nm.

(AFM). The pattern is composed of parallel lines that replicate the periodicity of the stamp. At greater magnification the thickness of the lines is not homogeneus (100 ± 20 nm) and occasionally seem to be fragmented into smaller islands. Comparison of the stamp motif and the printed pattern indicates that the protrusion motifs have been reproduced and reduced in size (~10%). The size of the printed lines in this particular case is about 500 nm width with a pitch of 1.5 μm. Phase imaging and lateral force imaging show strong compositional contrast between the printed lines and the space separating them, suggesting that there is no material deposited between the lines.

In order to transform the patterned low-temperature molecule-based magnet into the room-temperature magnetic oxide and detect the magnetic response, the substrate was transferred into an oven at 450 °C, heated to 600 °C, and afterward studied with a magnetic force microscope (MFM). Figure 13 shows MFM images of the patterned material after thermal decomposition acquired at room temperature. The strong contrast observed indicates the magnetic nature of the nanostructured material. The magnetic pattern is composed of lines with sizes similar to those before the thermal treatment. A closer look reveals that these lines are composed of nanometric spots, probably formed from segregation of the prepatterned material during the thermal treatment. To prevent this point, we are currently exploring more gentle thermal treatments. Additionally, we are currently working in the organization of room-temperature magnetic nanometric dots by controlling the distance between the stamp and the substrate, using extremely dilute conditions, and modifying the stamp motif. The employment of an alternative scanning probe lithography (SPL) such as dip-pen nanolithography (DPN) is also being tested.

Conclusions

In summary, we have presented the synthesis, structure, and magnetic characterization of a entire new family of layered

(37) (a) Cavallini, M.; Biscarini, F.; León, S.; Zerbetto, F.; Bottari, G.; Leigh, D. A. *Science* **2003**, *299*, 531. (b) Cavallini, M.; Bracali, M.; Aloisi, G.; Guidelli, R. *Langmuir* **1999**, *15*, 3003–3006. (c) Collier, C. P.; Wong, E. W.; Belohradsky, M.; Raymo, F. M.; Stoddard, J. F.; Kuekes, P. J.; Williams, R. S.; Heath, J. R. *Science* **1999**, *285*, 391–394. (d) M. Cavallini, M.; Aloisi, G.; Bracali, M.; Guidelli, R. J. *Electroanal. Chem.* **1998**, *444*, 75–81.

polymetallic "cation-less" oxalate-bridged layered 2D magnets with the general formula $[M^{II}(H_2O)_2]_3[M^{III}(ox)_3]_2(18\text{-crown-}6)_2$ (M^{III} = Cr, Fe; M^{II} = Mn, Fe, Co, Ni) (**1**−**8**). These compounds exhibit long-range magnetic ordering at low temperatures. Among them, those built up from $[Cr(ox)_3]^{3-}$ complexes behave as ferromagnets with critical temperatures up to 8 K, whereas the $[Fe(ox)_3]^{3-}$ series present ferrimagnetic ordering up to 20 K. These results indicate that supramolecular interactions, such as hydrogen bonding, can also play an important role to promote and control the dimensionality and magnetic response of molecule-based magnets, as has already been explored with cation/anion electrostatic interactions or the employment of capping ligands. We also note the solubility of these compounds in water and polar solvents, in comparison with the insolubility of the majority of oxalate-based coordination frameworks reported up to date. This property, rarely found in magnets formed by extended networks,[26] is common for the rest of crown ether containing magnetic CPs developed by our group.[12,13,31] Although the magnetic properties of the original solids are obviously not retained in solution, evaporation of the solvent or precipitation through the addition of nonpolar solvents can easily regenerate the original CPs. This point allows for the production of large good-quality single crystals, which will permit us in the near future to carry out single-crystal magnetic characterization, providing a deeper understanding of the magnetism in these systems.

We have also discovered how the controlled thermal decomposition of these oxalate-based molecular magnets yields single-phase spinel-like mixed oxides (**9**−**14**), which exhibit ferrimagnetic ordering at temperatures higher than those of their molecular precursors. Among them, special attention has been paid to **14**, which behaves as a magnet at room temperature. This strategy presents two advantages with respect to the standard ceramic method, which generally relies on the decomposition of mechanically homogenized mixtures of simple metallic salts:[38] (a) the oxide is formed at lower temperatures (ca. 450 °C); (b) the thermal decomposition of a preassembled framework of metallic ions will result in higher homogeneity of the resulting oxide, preventing the appearance of contaminant phases; (c) the versatility of the chemical approach will permit accessing a broad number of intermetallic oxides by tuning the stoichiometry and composition of the molecular precursor.

Taking advantage of the solubility of these materials, we have accomplished the patterning of **6** onto Si(110) at the submicrometric scale and studied the magnetic response of the nanostructured oxide resulting from its thermal decomposition. This chemical approach involves the patterning of the molecular precursor onto a solid substrate through the LCW technique. In a posterior step, the material incorporated to the substrate can be thermally decomposed, producing a large-area nanopatterning of the magnetic oxide in a few seconds and in a single step (fast and easy). Note that this is one of the main requirements for a possible technological transfer to satisfy the increasing demand of higher area density magnetic storage, as foreseen by Kryder's law.[39]

This work paves the way for the employment of these soluble precursors of magnetic oxides to develop a wide range of new applications that were not possible up to now, due to the poor solubility of the molecular precursors employed in the classical synthesis of mixed oxides by thermal treatment. In this direction, we are currently working on the design of water-soluble inks and their organization into arrays of micro-/nanometric dots by means of inkjet printing or other nanolithographic techniques such as DPL. These functional patterns will be useful in ceramics as well as in the development of high-density magnetic patterned memories as an alternative to the conventional granular continuous magnetic thin film media.[40] Furthermore, the synthetic versatility of this chemical approach, in contrast with those typically designed from a "top-down" physical point of view, should permit modifying the stoichiometry and nature of the metallic ions in the assembled CP, thus tuning the chemical composition of the resulting oxide and consequently its physical properties. In this direction, we are currently investigating the incorporation of Mn, Ln, and alkaline-earth ions into related CPs in order to accomplish an important technological challenge: the production of nanometric Manganite phases leading to colossal magnetoresistance (CMR) based high-density devices.[41]

Acknowledgment. Financial support from the EU (MolSpinQIP and the ERC Advanced Grant SPINMOL), the Spanish Ministerio de Ciencia e Innovación (Project Consolider-Ingenio in Molecular Nanoscience and projects MAT2007-61584 and CTQ-2008-06720), and the Generalitat Valenciana (Prometeo Program) are gratefully acknowledged. J.R.G.-M. and M.C. thank the CTQ-2008-03197/BQU and ESF-EURYI-DYMOT projects, respectively, for financial support. We also acknowledge J. M. Martínez Agudo for his help with the magnetic measurements.

Supporting Information Available: Tables and figures giving further details concerning the EDAX analysis, FT-IR studies, X-ray powder diffraction, and additional magnetic characterization of the compounds here reported. This material is available free of charge via the Internet at http://pubs.acs.org.

JA100261Z

(38) For examples of the methodology traditionally employed in the synthesis of spinels see: (a) Schiessl, W.; Potzel, W.; Karzel, H.; Steiner, M.; Alvius, G. M.; Martin, M.; Krause, K.; Halevy, I.; Gal, J.; Schäfer, W.; Will, W.; Hillberg, M.; Wäppling, R. *Phys. Rev. B* **1996**, *53*, 9143–9152. (b) Ma, Y.; Bahout, M.; Peña, O.; Durán, P.; Moure, C. *Bol. Soc. Esp. Ceram. Vidrio* **2004**, *43*, 663–667. (c) Laberty, C.; Alphonse, P.; Demai, J. J.; Sarda, C.; Rousset, A. *Mater. Res. Bull.* **1997**, *32*, 249–261.

(39) Walter, C. *Sci. Am.* **2005**, *293*, 32–33.

(40) Coronado, E.; Martí-Gastaldo, C.; Galán-Mascarós, J. R. Polímeros de coordinación solubles homo y heterometálicos basados en el ligando oxalato y método de obtención de espinelas a partir de ellos. Patent WO2009130359-A1.

(41) Loudon, J. C.; Mathur, N. D.; Midgley, P. A. *Nature* **2002**, *420*, 797–800.

(42) Atovmyan, L. O.; Shilov, G. V.; Lyubovskaya, R. N.; Zhilyaeva, E. I.; Ovanesyan, N. S.; Pirumova, S. I.; Gusakovskaya, I. G. *JETP Lett.* **1993**, *58*, 766–769.

(43) Coronado, E.; Galán-Mascarós, J. R.; Gómez-García, C. J.; Ensling, J.; Gütlich, P. *Chem. Eur. J.* **2000**, *6*, 552–563.

(44) Decurtins, S.; Schmalle, H. W.; Oswald, H. R.; Linden, A.; Ensling, J.; Gutlich, P.; Hauser, A. *Inorg. Chim. Acta* **1994**, *216*, 65–73.